Evidence of defect-induced polarization clusters in nominally pure $KTaO_3$ from low-temperature Raman and hyper-Raman spectra

1991 J. Phys.: Condens. Matter 3 3697

(http://iopscience.iop.org/0953-8984/3/21/003)

J. Phys.: Condens. Matter 3 (1991) 3697–3709. Printed in the UK

Evidence of defect-induced polarization clusters in nominally pure $KTaO_3$ from low-temperature Raman and hyper-Raman spectra

H Vogt

Max-Planck-Institut für Festkörperforschung, Heisenbergstrasse 1, D-7000 Stuttgart 80, Federal Republic of Germany

Received 7 January 1991

Abstract. A comparison is made between low-temperature Raman and hyper-Raman spectra of six single crystals of $KTaO_3$ grown as pure according to the present state of the art by top-seeded solution and spontaneous-nucleation techniques. All samples differ in four spectral features: (a) first-order Raman intensity, (b) hyper-Rayleigh intensity, (c) width of the soft-mode hyper-Raman line, (d) soft-mode frequency. While (a), (b) and (c) are approximately linear functions of each other, (d) turns out to vary with the square of (a) or (b). No correlation is found between any of the four quantities under study and the photoluminescence at 687 nm recently assigned to Ta^{3+} near oxygen vacancies. The results are interpreted in terms of polarization clusters formed by the host crystal in response to static or quasi-static defects of the random local-field type. Since the radius of a single polarization cluster reaches the magnitude of about five lattice constants, the specific defect structure at the centre is screened, so that the observed relationships between (a), (b), (c) and (d) become rather general.

1. Introduction

Static or quasi-static lattice distortions around defects are usually described in terms of the phonon Green's function of the host crystal [1]. Since the contribution of each phonon to this function embodies the square of the reciprocal phonon frequency, optic-phonon-type distortions do not play a major role compared to the elastic or acoustic-phonon-type ones, provided the influence of the long-range electric fields due to the charge distribution of the defects can be neglected [2]. While the optic-phonon-type distortions fade away within a few lattice constants, the elastic ones slowly decrease with increasing distance r from the defect, the asymptotic behaviour of the elastic displacement field being characterized by r^{-2} [1, 2]. A somewhat intermediate situation is encountered when the soft-mode component is extracted from the lattice distortion induced by a defect in a ferroelectric material near its phase transition [3]. In the simplest approximation the static or quasi-static soft-mode polarization $\hat{P}(r)$ surrounding a point defect of appropriate symmetry in the paraelectric phase is given by

$$\hat{P}(r) = \hat{P}(d)\frac{d}{r}\exp[-(r-d)/r_c] \qquad (r > d) \tag{1}$$

0953-8984/91/213697+13$03.50

where d and r_c are the radius of the defect core and the correlation radius of the soft-mode polarization, respectively. In general, d has the order of magnitude of a lattice constant and may be assumed to be independent of temperature, whereas r_c is proportional to the inverse of the soft-mode frequency Ω_0 and tends to diverge near the phase transition point, i.e. [5]

$$r_c \sim \Omega_0^{-1}. \tag{2}$$

Various names, sometimes with subtle distinctions, have been given to the phenomenon specified by equations (1) and (2), e.g. polarized clusters [6], ferroelectric microregions or microdomains [7] and frozen-in fluctuations of the order parameter [4]. Such concepts have been used extensively in order to explain various anomalous features in light scattering spectra, especially the appearance of symmetry forbidden Raman lines and elastic or quasielastic central peaks [8, 9].

In a recent communication [10] (hereafter referenced as I) second-harmonic light or hyper-Rayleigh (HRL) scattering from the bulk of nominally pure $KTaO_3$ has been investigated as a function of scattering geometry and temperature between 10 and 200 K. Interrelations between HRL and soft-mode hyper-Raman (HRM) scattering have been observed which become particularly transparent at low temperatures ($T < 50$ K). (i) The HRL intensity varies with temperature as Ω_0^{-4}. (ii) The HRL selection rules on the polarizations of incident and scattered light are determined by the soft-mode HRM tensor although in a slightly different way than the selection rules of the soft-mode HRM scattering itself.

The Ω_0^{-4} law follows from the assumption that non-interacting clusters, polarized according to equation (1), contribute incoherently to the HRL signal, each contribution being proportional to the square of the volume integral of $\hat{P}(r)$ and hence to the fourth power of r_c or Ω_0^{-1}. Consistently, the HRL selection rules can be deduced from the derivative $\partial\chi^{(2)}/\partial\hat{P}$ of the second-order susceptibility $\chi^{(2)}$ of the host crystal with respect to $\hat{P}$ at $\hat{P} = 0$, i.e. from the soft-mode HRM tensor [11]. An appropriate average of the square of $\partial\chi^{(2)}/\partial\hat{P}$ has to be taken over the random distribution of directions in which the clusters are polarized. As long as the overall cubic symmetry of $KTaO_3$ is preserved, the result is quite independent of the particular distribution assumed.

In their effort to interpret previous reports on collinear second-harmonic generation (SHG) in paraelectric $KTaO_3$, $SrTiO_3$ and $BaTiO_3$, Prusseit-Elffroth and Schwabl [12] have come to similar conclusions and to findings in line with (i) and (ii).

The present paper intends to answer several questions left open in I. First, the polarization clusters probed by HRL scattering are shown definitely to arise from defects and not from quasi-static intrinsic odd-parity excitations like hopping motions between off-centre positions of the Ta ions. Secondly, the intensity of first-order Raman (FOR) scattering is found to correlate with the intensity of HRL scattering, so that speculations about a common origin of both effects are confirmed. Thirdly, HRM spectroscopy proves to be capable of detecting variations of the soft-mode damping constant and frequency accompanying the variations of FOR and HRL intensities. During the course of this work, reports on photoluminescence from $KTaO_3$ around 687 nm [13, 14] have offered the possibility to single out oxygen vacancies as the only defect core of the polarization clusters in nominally pure samples. Hence we have supplemented our measurements by a search for correlations between the photoluminescence on the one side and FOR, HRL and soft-mode HRM scattering on the other. Our negative result

indicates that in our samples the particular defects traced by the photoluminescence either do not induce polarization clusters at all or are exceeded in this respect by others. Recent observations [14] of enhanced photoluminescence *and* FOR scattering from samples deliberately reduced in a hydrogen atmosphere at elevated temperatures favour the second alternative because they suggest a common origin of both effects under certain sample conditions. Nevertheless there is some probability that different defects are operative, only their concentrations being simultaneously increased during the reduction procedure.

Our subject matter is divided into two sections. In section 2 we summarize theoretical concepts and expectations. In the interest of clarity we do not ponder on the various nomenclatures developed in the literature to describe the mutual influence of defects and host crystals near structural phase transitions. Instead, we mainly use the continuum approximation elaborated by Levanyuk *et al* [3,4,8,9]. In section 3 we present our experimental data and discuss how far they verify the predictions of section 2.

2. Theoretical background

2.1. Continuum approximation

In the continuum approximation the response of the $KTaO_3$ host crystal to defects is derived from the well known Landau expansion of the free energy density [4,9]

$$\Phi[P] = \tfrac{1}{2}AP^2 + \tfrac{1}{4}BP^4 + \tfrac{1}{2}D(\nabla P)^2 - gP^2x - \tfrac{1}{2}fP^2x^2 \tag{3}$$

where g and f represent electrostrictive coefficients and A, B and D have the standard meaning with $A \sim \Omega_0^2$. For the sake of simplicity, the purely elastic part of Φ is omitted and the soft-mode polarization or order parameter P as well as the elastic strain x are treated as scalars. Both quantities split into quasi-static defect-induced contributions $\hat{P}$, $\hat{x}$ and phonon contributions P', x', i.e. $P = \hat{P} + P'$ and $x = \hat{x} + x'$. As indicated by the spectral separation of the HRL and the soft-mode HRM lines (see I), $\hat{P}$ and P' refer to time scales differing by orders of magnitude. Hence any dynamic coupling between $\hat{P}$ and P' may be neglected.

Minimizing Φ, we obtain the following equations for $\hat{P}$ and P':

$$D\nabla^2\hat{P} - A\hat{P} = B\hat{P}^3 - (2g + f\hat{x})\hat{P}\hat{x} \tag{4}$$

$$D\nabla^2P' + A\left[\left(\frac{\Omega}{\Omega_0}\right)^2 - 1\right]P' = (3B\hat{P}^2 - 2g\hat{x} - f\hat{x}^2)P' + 2B\hat{P}(P')^2 - 2f\hat{P}\hat{x}x' - 2(g + f\hat{x})P'x' - f\hat{P}(x')^2. \tag{5}$$

The presence of a defect is modelled by the boundary conditions on the solutions of equation (4) at the interface between defect core and surrounding polarization cluster [4]. The Ornstein–Zernike function of equation (1) with $r_c^2 = D/A$ represents the lowest-order approach to this problem.

The experimental results of I suggest two restrictive and simplifying assumptions.

(a) Linear and planar defects are absent. Indeed, they would give rise to HRL scattering intensities varying with temperature as Ω_0^{-3} and Ω_0^{-2}, respectively. Within

the framework of the continuum description the observed Ω_0^{-4} dependence can be explained only by the presence of point defects.

(b) Below 50 K there is no restructuring of the defects or local phase transition. Moreover, the boundary value $\hat{P}(d)$ of the quasi-static soft-mode polarization at the defect-core/polarization-cluster interface is almost independent of temperature. This condition seems to be satisfied because otherwise the temperature dependence of the HRL intensity should deviate from the Ω_0^{-4} law.

The defects specified so far are referred to as stiff or frozen-in point defects [9]. They may be further characterized as symmetry-breaking defects of the random local-field type or as symmetry-conserving defects of the random local transition temperature type, the local phase transition to the symmetry-breaking defect structure having already occurred (soft-defect limit) [9,15]. In the Halperin–Varma classification scheme the defects under consideration are denoted by A2 or B2 [16].

In discussing the various coupling mechanisms activated by the polarization clusters we shall always approximate the solution of equation (4) by a sum of Ornstein–Zernike functions centred at randomly distributed defect sites. This sum will also be inserted into the right-hand side of equation (5) in order to account for the defect-induced damping and frequency shift of the zone-centre soft mode.

We note that equation (5) describes the dispersion of the soft phonon branch by the expression

$$\Omega^2(q) = \Omega_0^2\,(1 + r_c^2 q^2) \tag{6}$$

which specifies the extent to which the continuum description should be reproduced from exact lattice-dynamics calculations in the long-wavelength limit.

2.2. Hyper-Rayleigh scattering

According to I and the remarks of section 1, a comparison of the HRL scattering intensities from different samples of $KTaO_3$ should be based on the formula

$$I_{\mathrm{HRL}} \sim r_c^4 \sum_i \frac{N_i}{V}[d_i \hat{P}(d_i)]^2. \tag{7}$$

The sum over i indicates that a diversity of non-interacting defects is permitted, each defect i being characterized by its concentration N_i/V, core radius d_i and core-boundary polarization $\hat{P}(d_i)$. As a reference for I_{HRL} we may use the intensity of the soft-mode HRM line which is certainly much less influenced by the defects than I_{HRL}.

2.3. First-order Raman scattering

Due to the broken symmetry within the polarization clusters, the optical phonons around the centre of the Brillouin zone become Raman active ([7] and references therein). The spectral Raman efficiency $S^{\sigma}_{\mathrm{FOR}}(\omega)$ of the optical phonon branch σ is determined by the power spectrum of the polarization

$$P^{\sigma}_{\mathrm{FOR}} = \sum_q \frac{\partial^2 \chi^{(1)}}{\partial \hat{P}(q) \partial Q^*_{\sigma}(q)} \hat{P}(q) Q^*_{\sigma}(q) E_{\mathrm{L}} \tag{8}$$

where $\hat{P}(q)$ is the Fourier transform of $\hat{P}(r)$, $Q^*_{\sigma}(q) = Q_{\sigma}(-q)$ the normal coordinate of the phonon of branch σ and opposite wavevector $-q$, $\chi^{(1)}$ the linear or first-order

susceptibility and E_L the electric field of the incident laser radiation. Representing $\hat{P}(r)$ by Ornstein–Zernike functions, we obtain

$$S^{\sigma}_{\mathrm{FOR}}(\omega) \sim r_c^4 \left(\sum_i \frac{N_i}{V} [d_i \hat{P}(d_i)]^2 \right) \int \mathrm{d}q \, \frac{g_\sigma(\omega, q)}{(1 + r_c^2 q^2)^2} \tag{9}$$

where $g_\sigma(\omega, q)$ is the lineshape function of the phonon of normal coordinate $Q_\sigma(q)$ and the sum over q has been replaced by an integral. On the basis of equation (9) three phenomena can be predicted, namely (a) as phonons with $q \neq 0$ are Raman activated, the defect-induced FOR lines are broader than the corresponding HRM lines the widths of which are given by $g_\sigma(\omega, 0)$; (b) the integral intensities $I^{\sigma}_{\mathrm{FOR}}$ of the FOR lines vary with temperature proportionally with $r_c \sim \Omega_0^{-1}$ as follows immediately from an integration of expression (9) over ω (see also the discussion about the correct power law in [9]); and (c) at a given temperature, $I^{\sigma}_{\mathrm{FOR}}$ is proportional to I_{HRL} for any σ.

2.4. Soft-mode damping

The damping mechanisms of the zone-centre soft mode follow from the terms on the right-hand side of equation (5). Since we are only concerned with low-temperature measurements, we can exclude all difference processes requiring the annihilation of a thermally activated phonon. Thus we neglect $2B\hat{P}(P')^2$ and $-2(g + f\hat{x})P'x'$. The second term stands for an electrostrictive process in which the zone-centre soft mode ($q_1 = 0$) absorbs a transverse acoustic phonon ($q_2 \neq 0$) to produce a higher-frequency phonon of the soft phonon branch ($q_3 = q_2 \neq 0$). This process has been considered to dominate the damping of the soft mode in pure $KTaO_3$ at elevated temperatures [17] and may be enhanced by the defect-induced strain field $\hat{x}$.

At low temperatures, the damping of a zone-centre transverse optic phonon is usually attributed to its decay into two or more acoustic phonons. Within the limits of the continuum approximation the decay of the soft mode into two phonons is symmetry-forbidden in pure $KTaO_3$. However, it is activated if polarization clusters are present, the corresponding term on the right-hand side of equation (5) being $-f\hat{P}(x')^2$. We may slightly generalize this argument by referring to the well known expressions obtained for the phonon self-energy in lowest-order perturbation theory [18]. The additional defect-induced damping function $\gamma^{(2)}_{\hat{P}}(\omega)$ may be written as

$$\gamma^{(2)}_{\hat{P}}(\omega) \sim \sum_q \sum_{\substack{q_1, q_2 \\ \sigma_1, \sigma_2}} \frac{1}{\omega_1 \omega_2} \left| \Phi^{(4)} \begin{pmatrix} 0 & q & q_1 & q_2 \\ \sigma_0 & \sigma_0 & \sigma_1 & \sigma_2 \end{pmatrix} \hat{Q}_{\sigma_0}(q) \right|^2 \Delta(q + q_1 + q_2)$$
$$\times \{\delta(\omega - \omega_1 - \omega_2) - \delta(\omega + \omega_1 + \omega_2)\} \tag{10}$$

where the coupling parameters $\Phi^{(4)}$ are fourth-order coefficients in the expansion of the potential energy Φ in terms of phonon normal coordinates. The quasi-static distortions within the polarization clusters are taken into account by the frozen-in normal coordinates $\hat{Q}_{\sigma_0}(q)$ of the soft phonon branch. The pairs (ω_1, ω_2), (q_1, q_2) and (σ_1, σ_2) denote the frequencies, wavevectors and branches of the acoustic phonons involved in the summation processes, respectively. The function $\Delta(q + q_1 + q_2)$ takes care of momentum conservation, while the difference of the two δ-functions guarantees that energy is conserved and $\gamma^{(2)}_{\hat{P}}(\omega)$ becomes an odd function of ω [18].

In the joint density of states description, equation (10) reduces to

$$\gamma_{\hat{P}}^{(2)}(\omega) \sim \sum_{q} |\Phi^{(4)}(q)\hat{Q}_{\sigma_0}(q)|^2 \rho^{(2)}(q,\omega) \tag{11}$$

where $\Phi^{(4)}(q)$ is an appropriate average of

$$\frac{1}{\sqrt{\omega_1\omega_2}}\Phi^{(4)}\begin{pmatrix} 0 & q & q_1 & q_2 \\ \sigma_0 & \sigma_0 & \sigma_1 & \sigma_2 \end{pmatrix}$$

over q_1, q_2 and $\rho^{(2)}(q,\omega)$ stands for the two-phonon density of states calculated in compliance with $\Delta(q + q_1 + q_2)$.

A further coarse reduction of equation (11) to essential factors yields

$$\gamma_{\hat{P}}^{(2)}(\omega) \sim f^2\langle|\hat{P}(q)|^2\rangle\rho^{(2)}(\omega) \sim f^2 r_c\Big(\sum_i \frac{N_i}{V}[d_i\hat{P}(d_i)]^2\Big)\rho^{(2)}(\omega). \tag{12}$$

The angle brackets indicate an average over the q-space, while $\rho^{(2)}(\omega)$ stands for the usual two-phonon density of states, i.e. $\rho^{(2)}(q = 0,\omega)$. Comparing equations (12), (7) and (9), we expect the soft-mode damping constant to vary linearly with I_{HRL} or I_{FOR}^{g} at any fixed low temperature because of the common factor $\sum_i N_i/V[d_i\hat{P}(d_i)]^2$.

The remaining terms on the right-hand side of equation (5), i.e. $-2f\hat{P}\hat{x}x'$ and $(2B\hat{P}^2 - 2g\hat{x} - f\hat{x}^2)P'$, describe quasi-harmonic couplings between the soft phonon branch and acoustic phonons and within the soft phonon branch itself. In the first case only acoustic phonons with frequencies around Ω_0 are relevant. They have wavevectors q at which $\hat{P}(q)$ is already so small that it cannot mediate the coupling between acoustic and optic phonons any longer. In the second case we may derive a damping function of the form

$$\gamma_{\hat{P}}^{(1)}(\omega) \sim B^2\langle|\hat{P}(q)|^4\rangle\rho^{(1)}(\omega) \sim B^2 r_c^5\Big(\sum_i \frac{N_i}{V}[d_i\hat{P}(d_i)]^2\Big)^2\rho^{(1)}(\omega). \tag{13}$$

Here we concentrate on the term $3B\hat{P}^2P'$ in equation (5) and introduce the one-phonon density of states $\rho^{(1)}(\omega)$ characterized by a M_0 critical point at $\omega = \Omega_0$ with $\rho^{(1)}(\Omega_0) = 0$.

Since the spectral width of the soft-mode HRM line is rather small, the measured damping constant γ is determined by the value of the damping function at $\omega = \Omega_0$. Thus, there is almost no contribution from $\gamma_{\hat{P}}^{(1)}(\omega)$ and the defect-induced increase of γ seems to be dominated by $\gamma_{\hat{P}}^{(2)}(\Omega_0) \sim I_{\mathrm{HRL}}$.

2.5. Shift of the soft-mode frequency

The defect-induced shift $\Delta\Omega_0$ of the soft-mode frequency Ω_0 has to be derived from the frequency-shift functions $\Delta(\omega)$ and $\Delta(\omega) + \Delta_{\hat{P}}(\omega)$ of $KTaO_3$ in the absence and presence of polarization clusters, respectively. A self-consistent description requires:

$$\Delta(\Omega_0) = 0 \qquad \Delta(\Omega_0 + \Delta\Omega_0) + \Delta_{\hat{P}}(\Omega_0 + \Delta\Omega_0) = 0. \tag{14}$$

Apart from frequency-independent contributions, $\Delta(\omega)$ and $\Delta_{\hat{P}}(\omega)$ are given by the *negative* Kramers–Kronig or Hilbert transforms of the corresponding damping functions, the density of states being the essential factors to be transformed [18].

If we assume that the soft-mode damping in pure $KTaO_3$ results from multiphonon processes, $\Delta(\omega)$ intersects the frequency axis at $\omega = \Omega_0$ with a slight negative slope. We may write

$$\Delta_{\hat{P}}(\Omega_0 + \Delta\Omega_0) = \left|\left(\frac{\partial\Delta}{\partial\omega}\right)_{\Omega_0}\right|\Delta\Omega_0 \approx 0. \tag{15}$$

The defect-induced frequency-shift function $\Delta_{\hat{P}}(\omega)$ splits according to

$$\Delta_{\hat{P}}(\omega) = \Delta_{\hat{P}}^{(0)} + \Delta_{\hat{P}}^{(1)}(\omega) + \Delta_{\hat{P}}^{(2)}(\omega) \tag{16}$$

where $\Delta_{\hat{P}}^{(1)}(\omega)$ and $\Delta_{\hat{P}}^{(2)}(\omega)$ follow from a Kramers–Kronig transformation of equations (13) and (12), respectively, while the frequency-independent contribution $\Delta_{\hat{P}}^{(0)}$ can be deduced directly from equation (5). We obtain

$$\Delta_{\hat{P}}^{(0)} = 3\pi r_c^3 \Omega_0 \frac{B}{D} \sum_i \frac{N_i}{V}[d_i \hat{P}(d_i)]^2 \tag{17a}$$

or, referring to the quartic anharmonic coupling parameters,

$$\Delta_{\hat{P}}^{(0)} \sim \frac{1}{\Omega_0} \sum_q \Phi^{(4)} \begin{pmatrix} 0 & 0 & q & -q \\ \sigma_0 & \sigma_0 & \sigma_0 & \sigma_0 \end{pmatrix} |\hat{Q}_{\sigma_0}(q)|^2. \tag{17b}$$

Both expressions describe the well known effect of the polarization-induced shift of the soft-mode frequency [19]. Usually, this effect is observed for a uniform quasi-static polarization $\hat{P}$ due to an externally applied electric field. In the case of a fluctuating $\hat{P}$ the frequency shift is determined by the average of $\hat{P}^2$ as shown by equation (17). Because of $B > 0$, $\Delta_{\hat{P}}^{(0)}$ is always positive as far as the strain-field corrections in equation (5) can be neglected.

At $\omega = \Omega_0 + \Delta\Omega_0$ the constant term $\Delta_{\hat{P}}^{(0)}$ in equation (16) is partly cancelled by

$$\Delta_{\hat{P}}^{(2)}(\omega) \sim -\int_0^\infty \frac{\rho^{(2)}(\omega')\,\mathrm{d}\omega'}{\omega' - \omega}. \tag{18}$$

This function becomes negative with a negative slope because the two-phonon density of states $\rho^{(2)}(\omega)$ contributes to the integral mainly above $\Omega_0 + \Delta\Omega_0$. Moreover, both $\Delta_{\hat{P}}^{(0)}$ and $\Delta_{\hat{P}}^{(2)}(\Omega_0 + \Delta\Omega_0)$ are proportional to $\sum_i N_i/V[d_i\hat{P}(d_i)]^2$ and hence to I_{HRL} or $I_{\mathrm{FOR}}^{\sigma}$.

Concerning $\Delta_{\hat{P}}^{(1)}(\omega)$, we realize that the negative Kramers–Kronig transform of the M_0 critical point of $\rho^{(1)}(\omega)$ yields a negative cusp proportional to Ω_0^{-1} [20]. If this structure is assumed to determine the zeroes of $\Delta_{\hat{P}}(\omega)$, we expect

$$|\Delta\Omega_0| \sim B^2 r_c^6 \left(\sum_i \frac{N_i}{V}[d_i\hat{P}(d_i)]^2\right)^2 \tag{19}$$

the sign of $\Delta\Omega_0$ being unpredictable on the basis of our arguments because it sensitively depends on the detailed balance of all three terms in equation (16). According to equation (18) $|\Delta\Omega_0|$ varies with the squares of I_{HRL} or $I_{\mathrm{FOR}}^{\sigma}$ at any fixed low temperature.

3. Experimental details and results

3.1. Samples and experimental set-up

Measurements are performed on six samples of nominally pure $KTaO_3$ grown in four different laboratories [21] by essentially two different techniques: the Czochralski-type top-seeded solution growth method (TSSG, samples No 2 and 6) [22] and the self-nucleation method based on the spontaneous formation of crystalline grains within a slowly cooled flux of Ta_2O_5 and K_2CO_3 (samples No 1, 3, 4 and 5) [23].

The samples are sawed and ground to cubes with {100} surfaces and 3 to 10 mm edge lengths. They are mounted in a Janis continuous-flow helium cryostat and cooled to 5 K.

Details of our HRM spectrometer have already been described in I. In order to measure ordinary Raman or photoluminescence spectra the Nd-YAG laser radiation is replaced either by its second harmonic or by the 5145 Å line of an Ar-ion laser.

3.2. Hyper-Raman spectra

Figure 1 shows the low-frequency Stokes part of the HRM spectrum obtained for two samples with almost the same incident laser intensity. The ratios I_{HRL}/I_{HRM} of the integral HRL and soft-mode HRM intensities differ by a factor of 2.5. Moreover, the larger value of I_{HRL}/I_{HRM} is associated with a broader HRM line at a higher frequency.

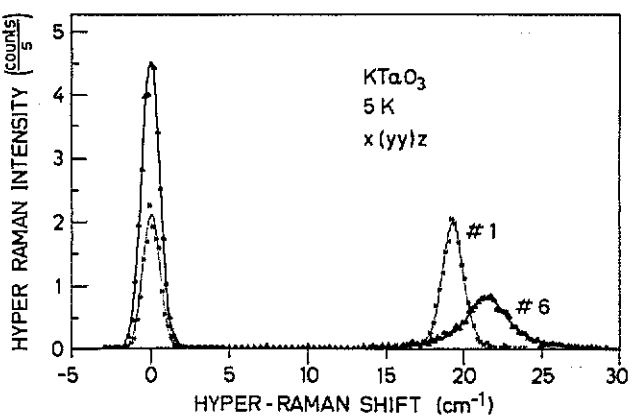

Figure 1. Hyper-Rayleigh and soft-mode hyper-Raman lines of two nominally pure samples of $KTaO_3$ at 5 K. Hyper-Rayleigh lineshape: instrumental profile of the spectrometer; hyper-Raman lineshape: convolution of the instrumental profile and a Lorentzian.

Some more details of the soft-mode behaviour are displayed in figure 2. The convolution of the Gaussian instrumental profile of the spectrometer and a Lorentzian is fitted to the experimental data points, all HRM lines being scaled to the integral intensity of sample No 1. We observe the damping of the soft mode to increase the more the soft-mode frequency deviates from an ideal value, either in the positive or in the negative direction. The full curve represents the soft-mode HRM line in the limit of a pure sample, the underlying damping constant γ and frequency Ω_0 being extrapolated from figure 7 (see subsection 3.5).

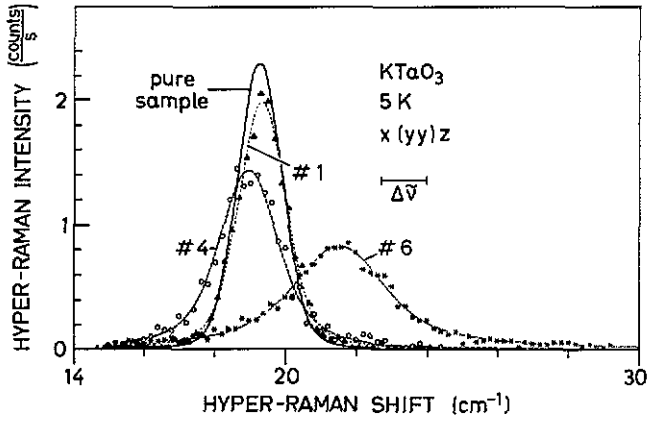

Figure 2. Soft-mode hyper-Raman lines of three nominally pure samples of $KTaO_3$ at 5 K. The bar $\Delta\tilde{\nu}$ indicates the spectral slit width. Full curve, extrapolation to the pure-sample limit according to figure 7: $\Omega_0 = 19.3\ cm^{-1}$, $\gamma = 0.2\ cm^{-1}$.

3.3. First-order Raman features

We restrict ourselves to the FOR features of the TO_4 phonon branch because it is the FOR feature that can most easily be separated from the intense second-order Raman background. In figure 3 we show the ordinary Raman spectra of three samples in the spectral range between 510 and 560 cm^{-1}. The second-order Raman background represents the lower-frequency shoulder of the $TO_4(X)$ + TA(X) sum band [24]. While the second-order Raman features of all samples coincide if referred to the same integrated Raman intensity, the FOR features do not. In order to extract the FOR intensity I^{σ}_{FOR} for $\sigma = TO_4$ from the measured spectrum, we fit the sum of a Lorentzian centred at 564 cm^{-1} and a second-degree polynominal to the second-order Raman background between 500 and 600 cm^{-1}, as indicated by the full curve in figure 3. $I^{TO_4}_{FOR}$ differs from sample to sample by almost the same factor as I_{HRL}/I_{HRM}.

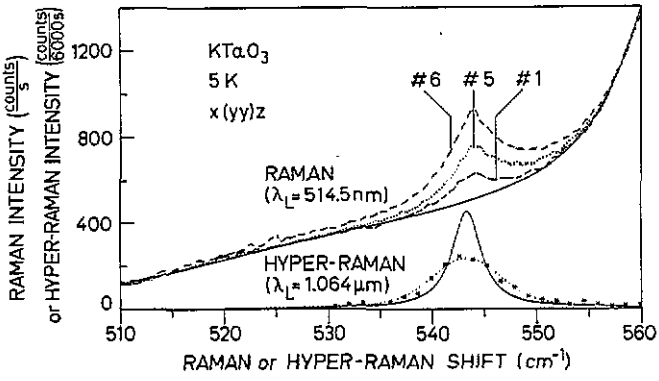

Figure 3. Upper curves, first-order Raman line of the TO_4 phonon branch superimposed on the lower-frequency shoulder of the $TO_4(X)$ + TA(X) sum band at 5 K. Lower curves, the measured (asterisks) and deconvoluted (full curve) hyper-Raman line of the zone-centre TO_4 phonon. Width of first-order Raman line, 5.2 cm^{-1}; width of the hyper-Raman line, 3.5 cm^{-1}.

For comparison, the measured and deconvoluted TO_4 HRM line is also plotted

in figure 3. Note that the FOR lines do not have to be deconvoluted because they refer to a spectral slit width of less than 1 cm^{-1}. In accordance to conclusion (a) in subsection 2.3 the width of the deconvoluted HRM line (full curve) is noticeably smaller than that of the FOR lines.

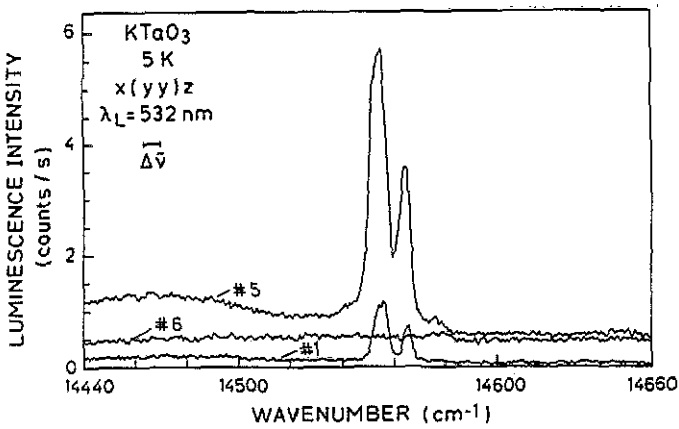

Figure 4. Zero-phonon lines of the red photoluminescence from three samples of $KTaO_3$ at 5 K excited by the second harmonic of the Nd-YAG laser. All spectra refer to the same second harmonic intensity. Note the absence of any correlation between the photoluminescence intensities and the first-order Raman intensities of figure 3.

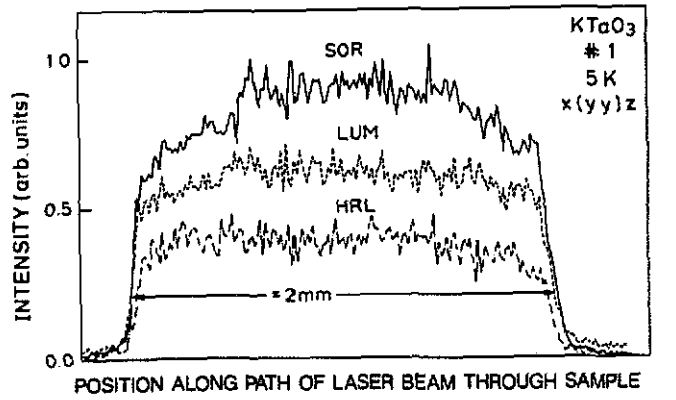

Figure 5. Second-order Raman (SOR), photoluminescence (LUM) and hyper-Rayleigh (HRL) intensities along the path of the laser beam through sample No 1. A 2 mm long section is cut out from this path by the entrance slit of the spectrometer.

3.4. Photoluminescence

Figure 4 presents the zero-phonon lines of the red photoluminescence around 687 nm excited by the second harmonic of the Nd-YAG laser. The spectra of the three samples refer to the same second-harmonic intensity. Comparing figure 4 with figures 1 and 3, we do not find any correlation between the photoluminescence intensity on the one hand and I_{HRL}/I_{HRM} or $I_{FOR}^{TO_4}$ on the other. This conclusion is also confirmed by figures 5 and 6, where second-order Raman, HRL and photoluminescence intensities along the path of the laser beam through the sample are plotted. Details of the experimental technique for obtaining such intensity distributions are described in I. The flat distributions of all intensities in figure 5 signify the homogeneity of the particular sample

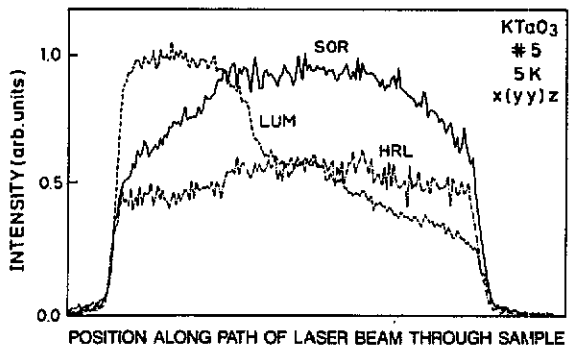

Figure 6. The same measurements as in figure 5 performed on sample No 5. The photoluminescence (LUM) curve indicates a gradient in the defect concentration.

under study. In figure 6, however, the photoluminescence curve indicates a gradient of the defect concentration. The uncorrelated behaviour of photoluminescence and HRL intensities excludes a common origin of both effects.

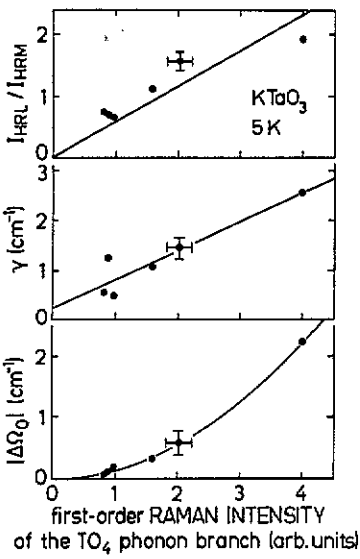

Figure 7. Ratio I_{HRL}/I_{HRM} of hyper-Rayleigh and soft-mode hyper-Raman intensities, soft-mode damping constant γ and soft-mode frequency shift $|\Delta\Omega_0|$ as functions of the first-order Raman intensity of the TO_4 phonon branch. In the previous figures the samples are numbered according to their sequence along the abscissa of this figure, i.e. in order of increasing first-order Raman intensity. The full lines and curves are fits of the linear and quadratic relationships predicted by equations (7), (9), (12) and (19) to the experimental points.

3.5. Relations between the foregoing results

In figure 7 the ratio I_{HRL}/I_{HRM} of HRL and soft-mode HRM intensities, the soft-mode damping constant γ, and the soft-mode frequency shift $|\Delta\Omega_0|$ are shown as functions of the FOR intensity $I_{FOR}^{TO_4}$ of the TO_4 phonon branch. Within the limitations set by the experimental accuracy and the small number of samples, our experimental results are in line with equations (7), (9), (12) and (19) predicting a linear relationship between I_{HRL}/I_{HRM}, γ and $I_{FOR}^{TO_4}$ as well as a quadratic dependence of $|\Delta\Omega_0|$ on $I_{FOR}^{TO_4}$.

4. Summary

In this paper we support the view that a nominally pure sample of $KTaO_3$ may be treated as a perfect crystal weakly perturbed by random local fields due to unavoidable defects. The analysis of the crystal response is divided into two steps. In the first step the formation of polarization clusters is considered. Their radius is determined by the soft-mode correlation length r_c and amounts to about five lattice constants at 5 K (see I), thus justifying the neglect of the specific defect structure at the centre. In the second step the quasi-static lattice distortions within the polarization clusters are regarded as sources of additional phonon coupling mechanisms based on quartic anharmonic coupling parameters and evidenced by an increased damping and a frequency shift of the zone-centre soft mode. Inclusion of HRM and second-order Raman susceptibilities yields HRL and FOR scattering.

In the limit of low defect concentrations the four quantities under study, i.e. I_{HRL}/I_{HRM}, $I_{FOR}^{TO_4}$, γ and $|\Delta\Omega_0|$ follow simple power laws with respect to both the correlation length r_c and the expression $\sum_i (N_i/V)[d_i\hat{P}(d_i)]^2$. In continuation of the present work an experimental verification of all of them is desirable.

Acknowledgments

The author wishes to thank M Cardona and J Kuhl for a critical reading of the manuscript and H Hirt, M Siemers and P Wurster for technical help. He is much indebted to S Jandl, S Kapphan, D Rytz, B Salce and H Uwe for providing samples of $KTaO_3$. The financial support of the Deutsche Forschungsgemeinschaft (Bonn, Federal Republic of Germany) is gratefully acknowledged.

References

[1] Ludwig W 1967 *Recent Developments in Lattice Theory (Springer Tracts in Modern Physics 43)* (Berlin: Springer) p 126
[2] Hardy J R and Lidiard A B 1967 *Phil. Mag.* **15** 825
[3] Levanyuk A P, Osipov V V and Sobyanin A A 1976 *Theory of Light Scattering in Condensed Matter* ed B Bendow, J L Birman and V M Agranovich (New York: Plenum) p 517
[4] Levanyuk A P, Osipov V V, Sigov A S and Sobyanin A A 1979 *Sov. Phys.-JETP* **49** 176
[5] Blinc R and Žekš B 1974 *Soft Modes in Ferroelectrics and Antiferroelectrics* (Amsterdam: North-Holland) p 34
[6] Höchli U T, Weibel H E and Boatner L A 1979 *J. Phys. C: Solid State Phys.* **12** L563
[7] Uwe H, Lyons K B, Carter H L and Fleury P A 1986 *Phys. Rev.* B **33** 6436
[8] Ginzburg V L, Levanyuk A P and Sobyanin A A 1980 *Phys. Rep.* **57** 151
[9] Levanyuk A P, Sigov A S and Sobyanin A A 1983 *Light Scattering near Phase Transitions* ed H Z Cummins and A P Levanyuk (Amsterdam: North-Holland) p 129
[10] Vogt H 1990 *Phys. Rev.* B **41** 11, 84; 1990 *Ferroelectrics* **107** 79
[11] Vogt H 1987 *Phys. Rev.* B **36** 5001
[12] Prusseit-Elffroth W and Schwabl F 1990 *Appl. Phys.* A **51** 361
[13] Grenier P, Bernier G, Jandl S, Salce B and Boatner L A 1989 *J. Phys.: Condens. Matter* **1** 2515
[14] Jandl S and Grenier P 1990 *Ferroelectrics* **107** 73
[15] Bruce A D and Cowley R A 1980 *Adv. Phys.* **29** 219
[16] Halperin B I and Varma C M 1976 *Phys. Rev.* B **14** 4030
[17] Barrett H H 1969 *Phys. Rev.* **178** 743
[18] Maradudin A A and Fein A E 1962 *Phys. Rev.* **128** 2589

See also modern textbooks on phonons, e.g. Brüesch P 1982, 1986 *Phonons: Theory and Experiments* vols I and II (Berlin: Springer)

[19] Fleury P A and Worlock J M 1968 *Phys. Rev.* **174** 613

[20] Cardona M 1969 *Modulation Spectroscopy* (New York: Academic) p 19; 1982 *Light Scattering in Solids* vol 2, ed M Cardona and G Güntherodt (Berlin: Springer) p 114

[21] Samples were provided by H Uwe, Institute of Applied Physics, University of Tsukuba, Japan (No 2), D Rytz, Sandoz Produkte AG, Basel, Switzerland (No 4, No 5), B Salce, Centre d'Etude Nucléaires, Grenoble, France (No 3), S Jandl, Département de physique, Université Sherbrooke, Canada (No 1) and S Kapphan, Fachbereich Physik, Universität Osnabrück, Federal Republic of Germany (No 6). Samples No 1 and No 3 were grown by L Boatner, Oak Ridge National Laboratory, USA.

[22] Belruss V, Kalnajs J, Linz A and Folweiler R C 1971 *Mater. Res. Bull.* **6** 899

[23] De Goër A M, Salce B and Boatner L A 1979 *Phonon Scattering in Condensed Matter* ed H J Maris (New York: Plenum) p 243

[24] Perry C H, Fertel J H and NcNelly T F 1967 *J. Chem. Phys.* **47** 1619